

Journal Pre-proof

Penetration-deflagration coupling damage performance of rod-like reactive shaped charge penetrator impacting thick steel plates

Tao Sun, Haifu Wang, Shipeng Wang, Jie Gong, Wenhao Qiu, Yuanfeng Zheng



PII: S2214-9147(25)00066-2

DOI: <https://doi.org/10.1016/j.dt.2025.02.027>

Reference: DT 1611

To appear in: *Defence Technology*

Received Date: 16 December 2024

Revised Date: 11 February 2025

Accepted Date: 27 February 2025

Please cite this article as: Sun T, Wang H, Wang S, Gong J, Qiu W, Zheng Y, Penetration-deflagration coupling damage performance of rod-like reactive shaped charge penetrator impacting thick steel plates, *Defence Technology*, <https://doi.org/10.1016/j.dt.2025.02.027>.

This is a PDF file of an article that has undergone enhancements after acceptance, such as the addition of a cover page and metadata, and formatting for readability, but it is not yet the definitive version of record. This version will undergo additional copyediting, typesetting and review before it is published in its final form, but we are providing this version to give early visibility of the article. Please note that, during the production process, errors may be discovered which could affect the content, and all legal disclaimers that apply to the journal pertain.

© 2025 China Ordnance Society. Publishing services by Elsevier B.V. on behalf of KeAi Communications Co. Ltd.

Penetration-deflagration coupling damage performance of rod-like reactive shaped charge penetrator impacting thick steel plates

Tao Sun^{a,b}, Haifu Wang^a, Shipeng Wang^c, Jie Gong^d, Wenhao Qiu^a, Yuanfeng Zheng^{a,*}

^aBeijing Institute of Technology, Beijing 100081, China

^bChina Aerospace Times Electronics Co., Ltd., Wuhan 430056, China

^cXi'an Institute of Electromechanical Information Technology, Xi'an 710065, China

^dHunan Vanguard Group Co., Ltd., Changsha 410028, China

*Corresponding Author: zhengyf@bit.edu.cn

Penetration-deflagration coupling damage performance of rod-like reactive shaped charge penetrator impacting thick steel plates

Abstract

The penetration-deflagration coupling damage performance of rod-like reactive shaped charge penetrator (RRSCP) impacting thick steel plates is investigated by theoretical analysis and experiments. A penetration-deflagration coupling damage model is developed to predict the penetration depth and cratering diameter. Four type of aluminum-polytetrafluoroethylene-copper (Al-PTFE-Cu) reactive liners with densities of 2.3, 2.7, 3.5, and 4.5 g·cm⁻³ are selected to conduct the penetration experiments. The comparison results show that model predictions are in good agreement with the experimental data. By comparing the penetration depth and cratering diameter in the inert penetration mode and the penetration-deflagration coupling mode, the influence mechanism that the penetration-induced chemical response is unfavorable to penetration but has an enhanced cratering effect is revealed. From the formation characteristics, penetration effect and penetration-induced chemical reaction behaviors, the influence of reactive liner density on the penetration-deflagration performance is further analyzed. The results show that increasing the density of reactive liner significantly increases both the kinetic energy and length of the reactive penetrator, meanwhile effectively reduces the weakened effect of penetration-induced chemical response, resulting in an enhanced penetration capability. However, due to the decreased diameter and potential energy content of reactive penetrator, the cratering capability is weakened significantly.

Keyword: Reactive materials; Al-PTFE composites; Penetration model; Damage effect

1. Introduction

The application of reactive liners in shaped charges breaks through the limitation of the single kinetic energy damage mode of traditional shaped charges with metal liners, and provides a new way for efficiently against armors and concrete fortifications [1,2]. Different from the traditional metal liner, this kind of reactive liner prepared by reactive materials (typical as aluminum-polytetrafluoroethylene composites) has both strength and energy attributes. More importantly, the reactive shaped charge penetrators (typical as reactive jets, rod-like reactive shaped charge penetrators (RRSCP)) formed by the reactive liners under the explosion drive not only have good kinetic energy penetration capability, but will also spontaneously induce deflagration reactions during penetration or after perforation. The damage capability could be dramatically enhanced by the combined effect of kinetic energy penetration and chemical energy release [3–6]. However, as an important characterization parameter of the terminal damage power of the shaped charge and an important basis for its structural optimization and design, the penetration-deflagration performance of reactive shaped charge penetrator has not been effectively predicted by model.

Existing research and design efforts are mainly based on experiments, which are relatively high cost-effectiveness ratio.

There are two major challenges in model prediction or research on the penetration-deflagration performance of reactive shaped charge penetrators. The key challenge is that the penetration-deflagration coupling damage process of reactive shaped charge penetrators involves complex dynamics, thermodynamics and thermochemistry, which is difficult to understand. Guo [7] proposed a reaction delay hypothesis in the study on the penetration-deflagration behavior of reactive jet. She considers that there is a time delay in the chemical reaction of the reactive jet during formation and penetration. Before this delay, the reactive jet remains inert and the damage mode is single kinetic energy penetration, but when the delay time is reached, the reactive jet immediately deflagrates completely, meanwhile the penetration terminates. Until now, most of the theoretical studies on the penetration-deflagration behavior of reactive shaped charge penetrators are based on the reaction delay assumption [7–10]. Combining the virtual origin model and penetration experiments, Guo [7] discussed the effects of standoff and reaction delay time on the penetration capability of reactive jet. Analysis shows that comparing with the standoff effect, the reaction delay time of reactive jet is the primary determinant of the penetration depth, showing a significant increase with the increase of the reaction delay time. Subsequently, Guo [8] found that the density of reactive jet showed a gradient distribution through numerical simulations and X-ray experiments. The linear distribution and deflagration pressure generated by each jet element at the bottom of crater are then introduced into the virtual origin model and the Bernoulli equation, respectively. Based on the modification, the analysis models for penetration depth and radial cratering of reactive jet are developed, and the penetration experiments of the reactive jet against steel plate are conducted to verify the validity of the model. In addition, it is [9] revealed that the wave shaper would increase the formation temperature rise of reactive jet and decrease the reaction delay time, resulting in a premature termination of penetration, which is unfavorable to penetration. Zheng [10] studied the chain damage effects of multi-spaced plates by reactive jet impact. The damage mechanism is revealed that the reactive jet produces mechanical perforations on the spaced plates by its kinetic energy, and then results in unusual chain rupturing effects and excessive structural damage on the spaced plates by its deflagration reaction. Then an analysis model is developed to discuss the rupturing damage behaviors. The analysis results show that the rupturing hole area on aluminum plates depends strongly upon the kinetic energy only-induced pre-perforations, the effective mass of the reactive jet, and the plate thickness. However, the reaction delay time, a key parameter used in these model calculations, needs to be obtained experimentally. Furthermore, the penetration-deflagration process of reactive shaped charge penetrators is actually a coupling effect of penetration and deflagration. However, the penetration-deflagration coupling interaction mechanism is not well understood, especially the influence mechanism of the penetration-induced chemical response on

the penetration and cratering, which is still unclear.

Another major challenge is that the penetration-deflagration coupling damage behaviors of reactive shaped charge penetrator are extremely complex, involving the comprehensive effects of various factors, such as the type of reactive shaped charge penetrator, the mechanically and chemically coupled formation characteristics and its material properties. Among them, the material density is an important mechanism to regulate the penetration-deflagration performance of reactive shaped charge penetrator [11]. From the existing published literature, the research object mainly focuses on the reactive jet, but there are relatively few studies on the RRSCP. Sun [12] observed through X-ray experiments that the reactive spherical segment liners can form excellent rod-shaped penetrators with tail skirts under the shaped charge effect. Based on the numerical simulation and thermal activation reaction theory, the composite formation structure characteristics of RRSCP composed of an inert-like leading reactive penetrator and a following chemical energy cluster is revealed. The unique composite formation structure allows the RRSCP to first perforate the aluminum plate by the leading reactive penetrator like a metal penetrator, and then release chemical energy by the following chemical energy cluster to cause further damage in a form of overpressure, resulting in a rupturing damage on the aluminum plate. In addition, the influence of the aluminum-polytetrafluoroethylene-copper (Al-PTFE-Cu) reactive liner density on the penetration capability of RRSCP is discussed from the formation point of view. Analysis shows that a higher liner density allows the Al-PTFE-Cu RRSCP to elongate more sufficiently, and greatly alleviates the negative effects of chemical reactions on the elongation, leading to a greater length-diameter ratio and thus significantly enhancing the penetration capability. Sun [13] also analyzed the penetration performance differences between reactive jet and RRSCP by comparing their formation morphologies, velocities, and activation reaction behaviors. It is pointed out that the chemical reaction of the activated material near the head and axis of the reactive jet will destroy the structural stability and cohesion of reactive jet during formation, which is unfavorable to penetration. Compared with the reactive jet, the shock reaction of RRSCP mostly occurs in the tail debris area, which has little effect on the overall performance of the penetrator and even the penetration capability. From the above studies, the research on the penetration-deflagration behaviors of RRSCP are not profound enough, especially the influence of the reactive liner density on the penetration-deflagration performance of RRSCP, which is not comprehensively analyzed.

In this paper, the theoretical model for the penetration-deflagration coupling damage performance is firstly developed and experimentally verified. Then, the influence mechanism of the penetration-induced chemical response on the penetration-deflagration performance is revealed by comparing the penetration depth and cratering diameter in the inert penetration mode and the penetration-deflagration coupling mode. Lastly, the influence of the Al-PTFE-Cu reactive liner density on the penetration-deflagration coupling damage performance of RRSCP is discussed at

three levels, namely, the formation characteristics, the penetration effect, and the penetration-induced chemical response behaviors.

2. Theoretical model for penetration-deflagration coupling damage

2.1. Description of penetration-deflagration process

Compared with the traditional metal shaped charge penetrator, the damage behavior of RRSCP impacting steel plates is more complicated. On the one hand, the formed RRSCP exhibits a unique composite structure composed of a leading reactive penetrator and a following chemical energy cluster, as shown in Fig. 1(a). Before impacting the plate, the leading reactive penetrator is inert-like, while the following chemical energy cluster will react and release chemical energy. This may trigger a morphology change of the reactive penetrator, and the effective mass of the reactive penetrator is difficult to evaluate. On the other hand, the reactive penetrator will be activated to react under the high penetration load, thus exhibiting a combined damage mode of kinetic penetration and chemical energy release. Furthermore, the RRSCP not only has an obvious velocity gradient, but also shows obvious temperature distribution characteristics, as shown in Figs. 1(b) and 1(c). This means that the activation reaction behaviors of each element in the reactive penetrator are different during penetration.

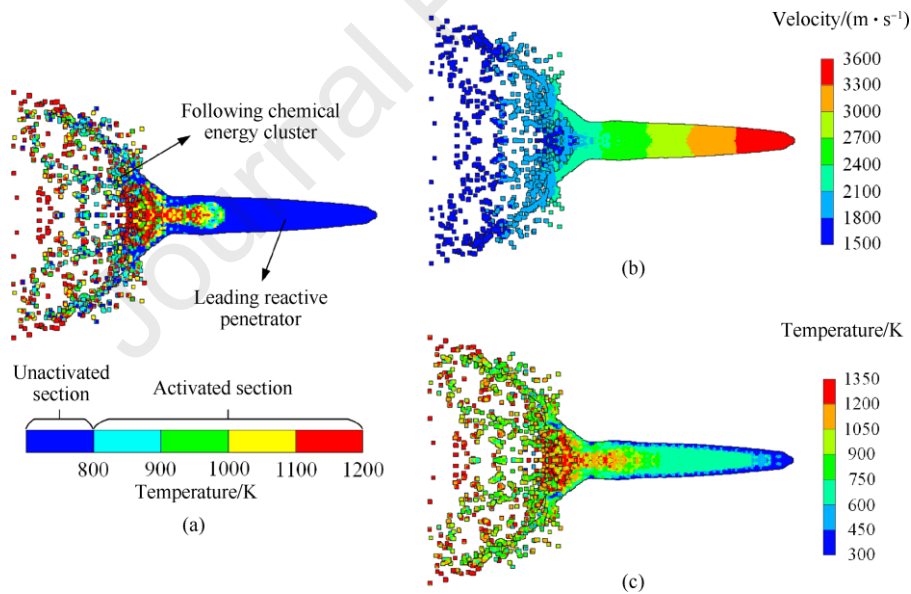


Fig. 1. Typical formation characteristics of RRSCP: (a) Composite structure feature; (b) Velocity distribution; (c) Temperature distribution.

In order to better understand the penetration-deflagration behaviors of RRSCP, its penetration-deflagration process is divided into three main stages, as shown in Fig. 2.

The first stage is the initial response stage, see Fig. 2(a). The RRSCP impacts the plate at high speed, producing two shock waves that propagate forward into the plate and backward into the reactive penetrator, respectively. The compressed reactive

materials and plate material experience high-strain-rate plastic deformation, and their temperatures rise sharply. At the same time, some reactive material debris ejects outward. Subsequently, a radial rarefaction wave is rapidly transmitted into the reactive penetrator, which causes the shock wave propagating in the reactive penetrator to stay near the impact interface. As a result, a stagnation shock wave in the reactive penetrator is formed. Between the stagnation shock wave and the impact interface, the reactive materials at high temperature, high pressure and high strain rate are activated to react, forming a chemical reaction zone. It should be pointed out that the duration of this stage is short, the penetration depth is small and the consumption of reactive penetrator is minimal.

The second stage is the steady penetration-deflagration stage, which is also the main stage, see Fig. 2(b). After the chemical reaction zone is formed, the subsequent reactive elements first experience a certain degree of chemical reaction and then impacts the steel plate. Under the strong impact compression, the shear deformation and fracture of reactive materials near the impact interface are caused, producing a large number of debris dispersing laterally along the hole wall. Meanwhile, the reactive material debris with larger specific surface and lower surface ignition energy will be ignited, which then expands rapidly to develop into deflagration. Subsequently, the plate material flows plastically and the penetration depth increases steadily under the combined effect of continuous kinetic energy penetration and chemical energy release of the reactive penetrator.

The third stage is the deflagration stage of the following chemical energy cluster into the penetration hole, see Fig. 2(c). As the leading reactive penetrator continues to penetrate, part of the following chemical energy cluster follows into the penetration hole along the penetration channel. When the reaction reaches a certain level or the secondary activation effect is caused by impact, the following chemical energy cluster deflagrates and releases chemical energy inside the penetration hole, resulting in an enhanced damage effect. It should be noted that when the standoff is large enough, the following chemical energy cluster has deflagrated before entering the penetration hole, so it will not contribute to the damage.

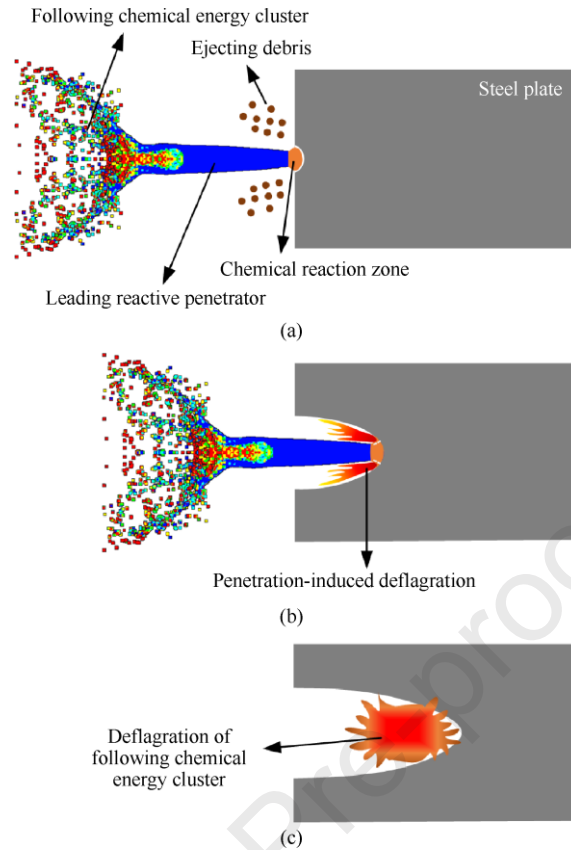


Fig. 2. Penetration-deflagration behavior of RRSCP impacting thick steel plate: (a) Initial response stage; (b) Steady penetration-deflagration stage; (c) Deflagration stage of following chemical energy cluster into penetration hole.

2.2. Penetration depth

As described in Section 2.1, the penetration-deflagration behavior of RRSCP is complex due to the coupled response mechanism of kinetic and chemical energy. In order to quantitatively analyze the penetration-deflagration coupling damage performance of RRSCP, the following assumptions are made:

(1) The influence of following chemical energy cluster on the formation of leading reactive penetrator is ignored.

(2) The initial response stage and the deflagration stage of following chemical energy cluster are ignored. It is considered that the steady penetration and deflagration occur when RRSCP impacts the plate.

(3) The shock wave effect in the plate is ignored.

(4) The reactive penetrator remains continuous without breaking in the penetration-deflagration process.

(5) The reactive penetrator is divided into n infinitesimal elements, and each reactive element is approximately a cylinder.

(6) There is always a stagnation shock wave during penetration.

The penetration-deflagration schematic diagram is shown in Fig. 3. The reactive penetrator in the steady penetration-deflagration process can be divided into three

parts: an undisturbed zone, a chemical reaction zone and a deflagration zone. Any element i in the undisturbed zone moves into the chemical reaction zone at a velocity of v_i , and then penetrates the steel plate after a certain degree of reaction. u is the penetration velocity. Subsequently, the element i radially disperses into the deflagration zone. δ is the width of the chemical reaction zone.

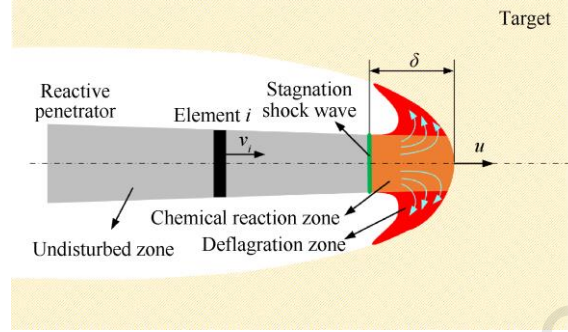


Fig. 3. Penetration-deflagration schematic diagram.

It is assumed that the reactive penetrator is a truncated conical rod and its velocity, temperature and diameter show linear distribution along the axial direction. When the reactive penetrator impacts the plate, the state of the element i can be expressed as:

$$\begin{cases} v_i = v_h - \frac{(v_h - v_w)}{L} \sum_1^{i-1} l_{0,i} \\ r_{0,i} = r_h + \frac{(r_w - r_h)}{L} \sum_1^{i-1} l_{0,i} \\ T_{0,i} = T_h + \frac{(T_w - T_h)}{L} \sum_1^{i-1} l_{0,i} \\ l_{0,i} = L/n \end{cases}, \quad i = 1, 2, \dots, n \quad (1)$$

where v_i , $r_{0,i}$, $T_{0,i}$ and $l_{0,i}$ are the velocity, radius, temperature and length of the element i when the reactive penetrator impacts the plate, respectively. v_h and v_w are the head and tail velocities of the reactive penetrator, respectively. r_h and r_w are the head and tail radii of the reactive penetrator, respectively. T_h and T_w are the head and tail temperatures of the reactive penetrator, respectively. L is the length of the reactive penetrator and n is the number of elements. The above initial parameters can be obtained by numerical simulation, see reference [12] for details.

When element i moves into the chemical reaction zone from the undisturbed zone, its pressure and temperature increase sharply, causing it to be activated to react. Subsequently, element i moves and reacts simultaneously until it impacts the plate. Based on the one-dimensional shock wave theory [14], the state of element i at the time of entering the chemical reaction zone can be expressed as:

$$V_{1,i} = \frac{C_j^2}{2s_j^2 P_{1,i}} \left[\sqrt{1 + \frac{4s_j V_0}{C_j^2} P_{1,i}} + \frac{2s_j (s_j - 1) V_0}{C_j^2} P_{1,i} - 1 \right] \quad (2)$$

$$T_{1,i} = T_{0,i} \exp\left[\frac{\gamma}{V_0}(V_0 - V_{1,i})\right] + \frac{V_0 - V_{1,i}}{2c_v} P_{1,i} + \frac{\exp\left[-\frac{\gamma}{V_0}(V_{1,i} - V_0)\right]}{2c_v} \int_{V_0}^{V_{1,i}} P_{1,i} \left[2 - \frac{\gamma}{V_0}(V_0 - V)\right] \exp\left[\frac{\gamma}{V_0}(V - V_0)\right] dV \quad (3)$$

where V and P are the specific volume and pressure, and the subscripts 0 and 1 denote the pre-wave and post-wave states, respectively. C_j and c_v are the sound speed and specific heat of reactive material, respectively. s_j and γ are the material coefficients. In this paper, the Al-PTFE-Cu reactive materials with different densities are studied and their shock parameters can be obtained by the method described in reference [12], as listed in Table 1.

Table 1

Shock parameters of Al-PTFE-Cu reactive materials with different densities [12].

| Materials | $\rho_0/(\text{g}\cdot\text{cm}^{-3})$ | $C_j/(\text{m}\cdot\text{s}^{-1})$ | s_j | γ | $C_v/(\text{J}\cdot\text{kg}^{-1}\cdot\text{K}^{-1})$ |
|-----------------------|----------------------------------------|------------------------------------|-------|----------|-------------------------------------------------------|
| Al-PTFE (0% Cu) | 2.3 | 2049 | 1.17 | 1.34 | 1006 |
| Al-PTFE-Cu (20% Cu) | 2.7 | 2267 | 1.23 | 1.46 | 764 |
| Al-PTFE-Cu (46.6% Cu) | 3.5 | 2640 | 1.3 | 1.6 | 579 |
| Al-PTFE-Cu (66% Cu) | 4.5 | 2998 | 1.36 | 1.72 | 492 |

The post-wave pressure $P_{1,i}$ of element i is actually caused by the impact of the previous element on the plate. Due to the small chemical reaction zone width and the continuous penetration process, the difference between the pressure of element i impacting the plate and the pressure of previous element impacting the plate is tiny. As an approximate replacement, the post-wave pressure $P_{1,i}$ can be expressed as [15]:

$$P_{1,i} = v_i \frac{\rho_{2,i} U_{s,i} \rho_t U_{t,i}}{\rho_{2,i} U_{s,i} + \rho_t U_{t,i}} \quad (4)$$

where $\rho_{2,i}$ is the density of element i when it moves to the penetration interface and ρ_t is the plate material density. For the 45# steel plate, the value of ρ_t is approximate 7.8 g/cm³. U_s and U_t are the propagation velocities of the shock wave in the reactive penetrator and the plate, respectively, which can be expressed as:

$$\begin{cases} U_{s,i} = C_j + s_j u_{j,i} \\ U_{t,i} = C_t + s_t u_{t,i} \end{cases} \quad (5)$$

where u_j and u_t are the particle velocities of the reactive penetrator and the plate, respectively. C_t is the sound speed of plate material and s_t is the plate material coefficient. The C_t and s_t of 45# steel plate are 4570 m/s and 1.49, respectively [16]. According to the following continuity conditions of interface pressure and velocity, the relationship between $P_{1,i}$ and $\rho_{2,i}$ can be obtained.

$$\begin{cases} v_i = u_{j,i} + u_{t,i} \\ \rho_{2,i} U_{s,i} u_{j,i} = \rho_t U_{t,i} u_{t,i} \end{cases} \quad (6)$$

When the shock temperature rise T_1 reaches the decomposition temperature of the PTFE matrix, the element i is activated to react. The reaction rate equation can be

written as [17]:

$$\frac{dy_i}{dt_i} = Z \exp\left(-\frac{E_c}{RT_{1,i}}\right) \cdot k (1-y_i) \left[-\ln(1-y_i)\right]^{\frac{k-1}{k}} \quad (7)$$

where y is the reaction extent, t is the reaction time, Z is the pre-exponential factor, E_c is the activation energy, R is the molar gas constant, and k is the coefficient related to the boundary conditions. It should be noted that the main reaction of Al-PTFE-Cu reactive materials is the reaction of the Al particles and PTFE matrix. For Al-PTFE compositions, the values of Z , E_c , R and k are $7.65 \times 10^{10} \text{ s}^{-1}$, 132.34 kJ/mol , $8.314 \text{ J}\cdot\text{mol}^{-1}\cdot\text{K}^{-1}$ and 1.5 , respectively [18,19]. The reaction time is approximately equal to the time that element i moves from the stagnation shock wave interface to the penetration interface (i.e., $t_i = \delta_i/v_i$). Integrating Eq.(7), we get:

$$y_i = 1 - \exp\left\{-\left[\frac{\delta_i}{v_i} \cdot Z \exp\left(-\frac{E_c}{RT_{1,i}}\right)\right]^k\right\} \quad (8)$$

Based on the propagation relationship between shock wave and rarefaction wave, the width of chemical reaction zone δ_i can be approximately expressed as:

$$\delta_i = \frac{r_{0,i}}{\sqrt{U_{R,i}^2 - U_{s,i}^2}} \cdot U_{s,i} \quad (9)$$

where U_R is the propagation velocity of radial rarefaction wave, which can be written as [20]:

$$U_{R,i} = U_{s,i} \sqrt{0.49 + \left(\frac{U_{s,i} - u_{j,i}}{U_{s,i}}\right)^2} \quad (10)$$

As a result of the chemical reaction, the density of element i decreases as it moves toward the penetration interface. When the element i moves to the penetration interface, its density $\rho_{2,i}$ can be approximately expressed as:

$$\rho_{2,i} = \frac{1 - (1-\eta)y_i}{V_{1,i}} \quad (11)$$

where η is the content of Cu. The density $\rho_{2,i}$ can be calculated by combining with Eqs.(2–11). It should be noted that Eqs.(2–11) involve a complex system of nonlinear equations, which should be solved by the iterative method.

Based on the Bernoulli equation, the penetration velocity u_i of element i can be expressed as [21]:

$$u_i = \frac{v_i - \sqrt{\frac{\rho_t}{\rho_{2,i}} v_i^2 + \left(1 - \frac{\rho_t}{\rho_{2,i}}\right) \frac{2R_t}{\rho_{2,i}}}}{1 - \frac{\rho_t}{\rho_{2,i}}} \quad (12)$$

where R_t is the plate resistance, which can be expressed as [22]:

$$R_t = \frac{2}{3} Y_t \left(1 + \ln \frac{2E_t}{3Y_t} \right) \quad (13)$$

where Y_t and E_t are the static yield strength and Young's modulus of plate material, respectively. For 45# steel plate, the values of Y_t and E_t are 355 MPa and 209 GPa, respectively [23]. Due to the velocity gradient, the reactive penetrator is gradually stretched during penetration. Based on the virtual origin theory, the length $l_{2,i}$ and radius $r_{2,i}$ of element i when it moves to the penetration interface can be expressed as:

$$\begin{cases} l_{2,i} = l_{0,i} + (v_i - v_{i+1}) \cdot \left(\sum_1^{i-1} H_i + \sum_1^{i-1} l_{0,i} \right) / v_i \\ r_{2,i} = \sqrt{l_{0,i} / l_{2,i}} \cdot r_{0,i} \end{cases} \quad (14)$$

where H_i is the penetration depth of element i , which can be expressed as [24]:

$$H_i = u_i \cdot \frac{l_{2,i}}{v_i - u_i} \quad (15)$$

Thus the penetration depth H_p of reactive penetrator can be obtained, which is expressed as:

$$H_p = \sum_{i=1}^n H_i = \sum_{i=1}^n \left(u_i \cdot \frac{l_{2,i}}{v_i - u_i} \right) \quad (16)$$

2.3. Radial cratering

The radial cratering of the reactive penetrator on the plate is actually a process in which pressure overcomes the plate strength and thus causes a radial plastic flow of plate material. Based on the coupling damage mechanism of kinetic energy penetration and chemical energy release, the radial cratering process can be divided into three stages, as shown in Fig. 4. First, the plate subjected to impact experiences shear deformation and fracture, forming an initial hole. The initial hole radius denotes r_f . Then, under the kinetic energy penetration pressure, the plate material overcomes the inertial force and flows at a high speed along the radial direction, achieving the secondary cratering. The corresponding cratering radius is increased to r_s . Finally, the third time cratering is produced by the deflagration of reactive materials. The ultimate cratering radius reaches r_b .

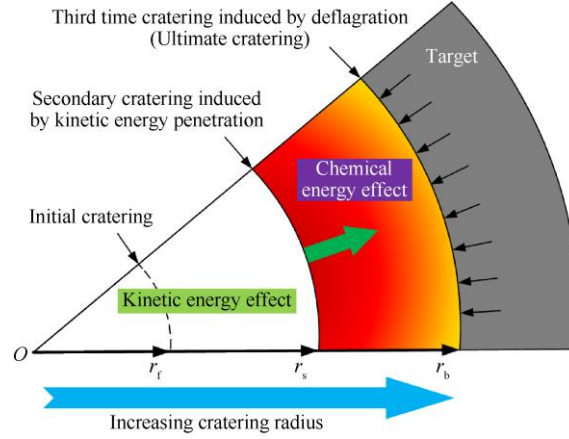


Fig. 4. Evolution process of cratering.

The initial hole radius r_f can be expressed as [24]:

$$r_{f,i} = \sqrt{2}r_{2,i} \quad (17)$$

The secondary cratering along the radial direction satisfies the Bernoulli equation [24].

$$P_{g,i} = \frac{1}{2}\rho_t u_{g,i}^2 + R_t \quad (18)$$

where P_g is the radial cratering pressure and u_g is the radial cratering velocity. According to Szendrei theory [25], radial cratering pressure decreases with increasing hole diameter, and the product of cratering pressure and cratering area is a constant.

$$P_{g,i} \cdot r_{g,i}^2 = P_{f,i} \cdot r_{f,i}^2 \quad (19)$$

where r_g is the cratering radius. P_f is the initial radial cratering pressure, which is equal to the axial penetration pressure.

$$P_{f,i} = \frac{1}{2}\rho_{2,i}(v_i - u_i)^2 \quad (20)$$

The radial cratering velocity u_g can be obtained by combining Eqs.(17–20), which can be expressed as:

$$u_{g,i} = \sqrt{\frac{2}{\rho_t} \left[\rho_{2,i}(v_i - u_i)^2 \frac{r_{2,i}^2}{r_{g,i}^2} - R_t \right]} \quad (21)$$

It can be found from Eq.(21) that the radial cratering velocity u_g decreases with an increase of cratering radius r_g . The secondary cratering terminates when the u_g decreases to zero. The secondary cratering radius r_s can be expressed as:

$$r_{s,i} = \sqrt{\frac{\rho_{2,i}(v_i - u_i)^2}{R_t}} \cdot r_{2,i} \quad (22)$$

The third time cratering triggered by the deflagration of reactive materials depends mainly on the properties of reactive material and plate material, which can be written as [5]:

$$r_{b,i} = \left(\frac{P_d}{2\sigma_d} \right)^{1/4} \cdot r_{s,i} \quad (23)$$

where P_d is the deflagration pressure of reactive materials and σ_d is the dynamic strength of plate material, which can be expressed as [5]:

$$\begin{cases} P_d = \frac{1}{4} \rho_0 D^2 \\ \sigma_d = Y_t \left[\frac{E_t (1-\mu)}{Y_t (1+\mu)(1-2\mu)} \right]^{1/4} \end{cases} \quad (24)$$

where D is the deflagration velocity of reactive materials and μ is the Poisson ratio of plate material. For 45# steel plate, the value of μ is taken as 0.3. According to the relevant experimental data, the deflagration velocity (m/s) of reactive materials is linearly negatively correlated with its density (g/cm^3) [5]. Their relationship can be approximately expressed as:

$$D \approx -553\rho_0 + 4545 \quad (25)$$

Combining Eqs.(22–25), the ultimate cratering radius r_b can be expressed as:

$$r_{b,i} = \left(\frac{\rho_0 (-553\rho_0 + 4545)^2}{8Y_t \left[\frac{E_t (1-\mu)}{Y_t (1+\mu)(1-2\mu)} \right]^{1/4}} \right)^{1/4} \cdot \sqrt{\frac{\rho_{2,i} (v_i - u_i)^2}{R_t}} \cdot r_{2,i} \quad (26)$$

3. Penetration experiments

3.1. Shaped charge with a liner made of reactive materials

The discussed shaped charge consists of explosive, a baffle ring, a reactive liner, a case, and a detonator, as shown in Fig. 5. The powerful explosive, 8701, is molded at a pressure of 200 MPa and initiated by the detonator. The density, diameter, and height of the explosive are 1.71 g/cm^3 , 50 mm, and 50 mm. The reactive liner is a spherical segment with an even wall thickness of 3 mm and a curvature radius of 45 mm. The 45# steel baffle ring is used to fix the reactive liner by gluing, and its inner and outer diameters are 45 mm and 50 mm, respectively. The 45# steel case thickness is 2 mm.

The fabrication method described in Reference [12] is used for the Al-PTFE-Cu reactive material liner. The fabrication process mainly includes powder mixing, molding, and sintering. First, Al, PTFE, and Cu powders are added to a ball mill at a certain mass ratio and mixed for 3 hours. It should be noted that the relative mass of Al and PTFE always follows the stoichiometric ratio of the chemical reaction under zero oxygen balance (i.e., 26.5 wt%: 73.5 wt%). The average particle diameters of the Al, PTFE, and Cu powders are 44 μm , 100 nm, and 24 μm , respectively. Then, the

uniform mixture is placed in a self-designed steel mold and pressed at a pressure of 200 MPa for 30 seconds. Third, the molded liner samples are sintered in a nitrogen-filled furnace at a maximum temperature of 380 °C. In this study, four types of Al-PTFE-Cu reactive material liners with Cu contents of 0%, 20%, 46.6%, and 66% are fabricated. The material compositions, densities and typical sample photographs are presented in Table 2.

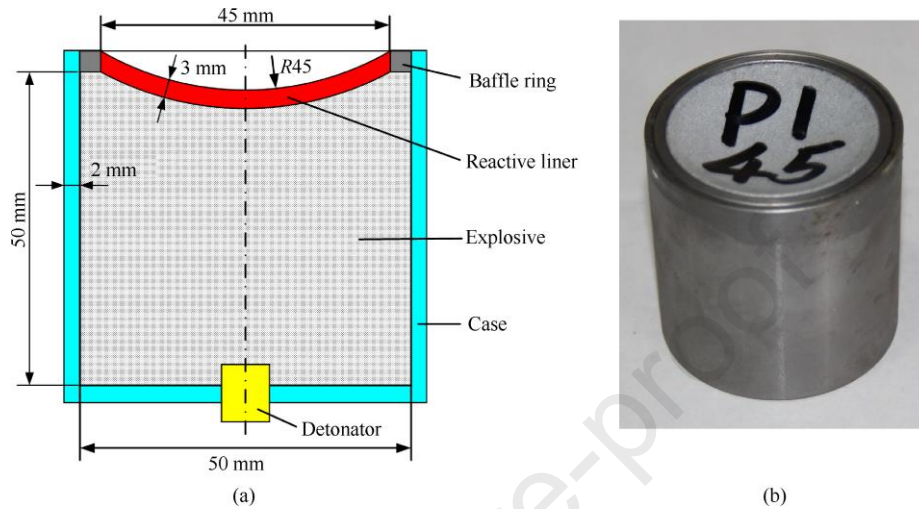


Fig. 5. Structure of shaped charge with reactive liner: (a) Schematic; (b) Typical physical photograph.

Table 2

Compositions, densities and photographs of fabricated reactive material liners.

| Material types | Material composition/(wt%) | | | Density/(g·cm ⁻³) | Typical sample photograph |
|----------------|----------------------------|------|------|-------------------------------|---------------------------------------------------------------------------------------|
| | Al | PTFE | Cu | | |
| P1 | 26.5 | 73.5 | 0 | 2.3 |  |
| P2 | 21.2 | 58.8 | 20 | 2.7 |  |
| P3 | 14.2 | 39.2 | 46.6 | 3.5 |  |
| P4 | 9 | 25 | 66 | 4.5 |  |

3.2. Experimental setup

The experimental setup is illustrated in Fig. 6. The shaped charge with the reactive liner is placed on a hollow standoff cylinder made of wood, and a 45# steel plate with a size of $\Phi 100 \times 100$ mm is placed below the standoff cylinder. The height of the standoff cylinder is three times the charge diameter (CD). After the charge is initiated, a RRSCP is formed and moves at a high velocity towards the steel plate. Then a penetration-deflagration damage is induced by impact.

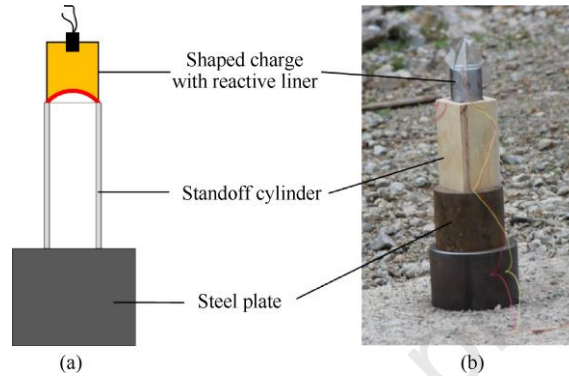


Fig. 6. Experimental setup: (a) Schematic; (b) Physical photograph.

4. Results and discussion

4.1. Comparison between experimental results and model calculations

Photographs of the damaged steel plates are shown in Fig. 7. It can be observed from Fig. 7(a) that the entrance holes basically present regular circular shapes. There are some smoke black marks distributed on the surface of the steel plate and the inner wall of the penetration hole, indicating that the RRSCP experiences a violent deflagration reaction during penetration. It can be found that from Fig. 7(b) that the penetration hole produced by the RRSCP with the lower density shows a regular funnel shape, and its inner wall is relatively smooth. The inner wall of penetration hole produced the RRSCP with the higher density is uneven. In addition, there are obvious purplish red Cu particles that not participated in the reaction.



Fig. 7. The damaged steel plates: (a) Entrance hole morphology; (b) Sectional views of

penetration holes.

Based on the simulation method in reference [12], the formation morphology of RRSCP at the time of impact is obtained, as shown in Fig. 8. The corresponding characteristic parameters (i.e., initial conditions for model calculation) of leading reactive penetrators are listed in Table 3. It should be noted that the tail temperature of the four types of reactive penetrators in Table 3 is the same, and all of them are 800 K. This is because the temperature of 800 K is the activation temperature threshold of the reactive materials [12], which is used to distinguish between the leading reactive penetrator and the following chemical energy cluster of RRSCP.

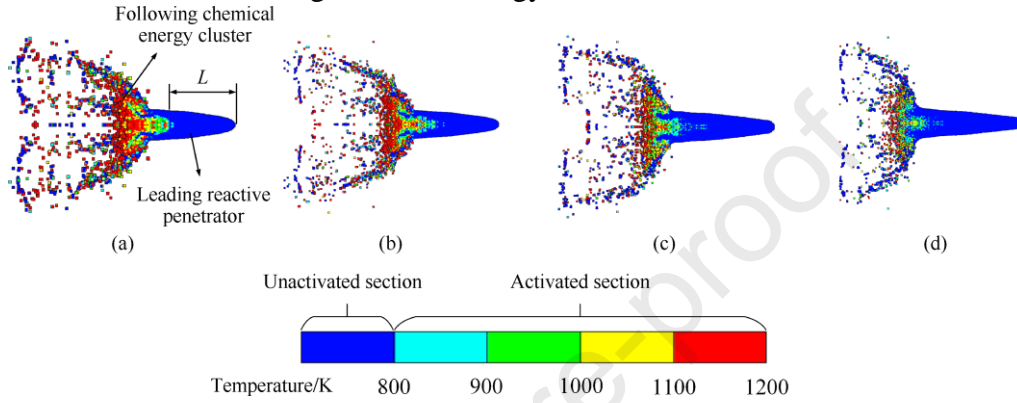


Fig. 8. The morphology of RRSCP at the time of impact: (a) $\rho_0 = 2.3 \text{ g}\cdot\text{cm}^{-3}$; (b) $\rho_0 = 2.7 \text{ g}\cdot\text{cm}^{-3}$; (c) $\rho_0 = 3.5 \text{ g}\cdot\text{cm}^{-3}$; (d) $\rho_0 = 4.5 \text{ g}\cdot\text{cm}^{-3}$.

Table 3

Characteristic parameters of leading reactive penetrators.

| $\rho_0/(\text{g}\cdot\text{cm}^{-3})$ | $V_h/(\text{m}\cdot\text{s}^{-1})$ | $V_w/(\text{m}\cdot\text{s}^{-1})$ | $v_h-v_w/(\text{m}\cdot\text{s}^{-1})$ | R_h/mm | V_w/mm | T_h/K | T_w/K | L/mm |
|----------------------------------------|------------------------------------|------------------------------------|----------------------------------------|-----------------|-----------------|----------------|----------------|---------------|
| 2.3 | 4550 | 3218 | 1332 | 4.2 | 6.2 | 415 | 800 | 47 |
| 2.7 | 4358 | 2955 | 1403 | 4 | 6.1 | 402 | 800 | 50 |
| 3.5 | 4002 | 2542 | 1460 | 3.7 | 6 | 343 | 800 | 53 |
| 4.5 | 3582 | 2243 | 1339 | 3.2 | 5.8 | 340 | 800 | 59 |

The experimental results and model calculations are listed in Table 4. The experimental data shows that the penetration depth is less than 1 CD and the entrance hole diameter is more than 0.5 CD, demonstrating that the RRSCP has a weak penetration capability but a strong cratering capability. Furthermore, the penetration-deflagration performance of RRSCP significantly depends on the reactive liner density. When the reactive liner density increases from $2.3 \text{ g}/\text{cm}^3$ to $4.5 \text{ g}/\text{cm}^3$, the penetration depth increases from 0.4 CD to 0.88 CD (an increase of more than 100%), while the entrance hole diameter decreases from 0.84 CD to 0.5 CD (a decrease of 40%). This indicates that the increasing reactive liner density significantly enhances the penetration capability of RRSCP, but significantly weakens its cratering capability. The calculated results show that as the reactive liner density increases from $2.3 \text{ g}/\text{cm}^3$ to $4.5 \text{ g}/\text{cm}^3$, the penetration depth increases from 0.35 CD to 1.14 CD and the entrance hole diameter decreases from 0.77 CD to 0.62 CD. Obviously, the model-predicted change trend of penetration depth and entrance hole diameter with reactive liner density is consistent with the experimental results, see Fig. 9. The

maximum errors of the model-predicted penetration depth and entrance hole diameter are 29.5% and 24%, respectively, which are less than 30%. This indicates that the model calculations are in good agreement with the experimental data. Therefore, the model can be used to quantitatively describe the penetration and cratering capabilities of RRSCP.

In comparison, the calculated results are lower than the experimental data when the reactive liner density is less than 2.7 g/cm^3 , and the calculated error decreases firstly and then increases with the increasing reactive liner density, and the calculated results are higher than the experimental data when the reactive liner density is more than 3.5 g/cm^3 . The reason would be that the reaction behavior of following chemical energy cluster and the reactive material density inhomogeneity effect caused by the chemical reaction are ignored in the model. On the one hand, more reactive materials at the rod tails of the formed RRSCP is activated to react when the reactive liner density is low, see Fig. 8. Then a larger expansion force will be produced within the leading reactive penetrator, which causes a weakened radial shrinkage effect during its free elongation, resulting in an increase of its diameter at the time of impact. As a result, the cratering capability will be enhanced. However, the activated reactive materials at the rod tail react incompletely at the standoff of 3 CD. In other words, this part of the reacting reactive materials still has a certain penetration capability, which is not considered in the model. Therefore, the calculated penetration depth and cratering diameter are lower than the experimental data when the reactive liner density is less than 2.7 g/cm^3 . On the other hand, the activated reactive materials at the rod tails gradually decreases as the reactive liner density increases, resulting in a decrease of its influence on the penetration-deflagration performance. In addition, under zero oxygen balance, the main reaction produced by Al-PTFE-Cu reactive element impact is the reaction of Al particle and PTFE matrix, while Cu almost does not participate in the reaction, see Fig. 7(b). As a result, the Al-PTFE-Cu reactive elements present density inhomogeneity or even non-condensation in the penetration-deflagration process, resulting in a decreased penetration pressure, which is unfavorable to penetration and cratering. As the reactive liner density increases, the Cu content increases continuously, which intensifies the influence of the penetration-induced chemical reaction on the compactness of reactive element, resulting in the further weakened penetration and cratering capabilities. Therefore, the calculated error decreases firstly and then increases with the increasing reactive liner density, and the calculated results are higher than the experimental data when the reactive liner density is more than 3.5 g/cm^3 .

Table 4

Comparison between experimental results and model calculations.

| No. | Liner density/($\text{g}\cdot\text{cm}^{-3}$) | Penetration depth (CD) | | | Entrance hole diameter (CD) | | |
|-----|-------------------------------------------------|------------------------|------------|--------|-----------------------------|------------|-------|
| | | Experimental | Calculated | Error | Experimental | Calculated | Error |
| 1 | 2.3 | 0.40 | 0.35 | -12.5% | 0.84 | 0.77 | -8.3% |

| | | | | | | | |
|---|-----|------|------|-------|------|------|-------|
| 2 | 2.7 | 0.44 | 0.43 | -2.3% | 0.80 | 0.74 | -7.5% |
| 3 | 3.5 | 0.66 | 0.74 | 12.1% | 0.68 | 0.72 | 5.9% |
| 4 | 4.5 | 0.88 | 1.14 | 29.5% | 0.50 | 0.62 | 24% |

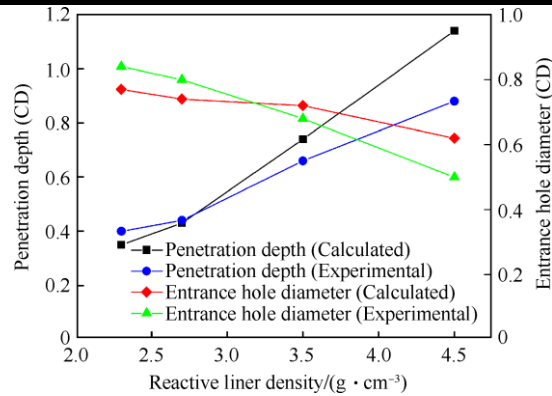


Fig. 9. Changing trends of penetration depth and cratering diameter with reactive liner density.

4.2. Influence of penetration-induced chemical response

As described in Section 2.1, the damage behavior of RRSCP on the steel plates is a complex penetration-deflagration coupling damage process. In order to reveal the influence mechanism of the penetration-induced chemical response on the penetration-deflagration performance, the penetration and cratering capabilities of the reactive penetrator in the inert penetration mode and the penetration-deflagration coupling mode are compared to analyze. The calculated model in the reference [25,26] is used as the inert penetration model. The No. 1 experimental condition in Table 3 is selected as the typical calculation condition.

The calculated results are shown in Fig. 10. In the inert penetration mode (without considering the chemical response), the penetration depth is 0.61 CD and the entrance hole diameter is 0.65 CD. Compared to the inert penetration mode, the penetration depth in the penetration-deflagration coupling mode is lower, which is 0.35 CD, but the entrance hole diameter is larger, which is 0.77 CD. This indicates that the penetration-induced chemical response is unfavorable to penetration but has an enhanced cratering effect.

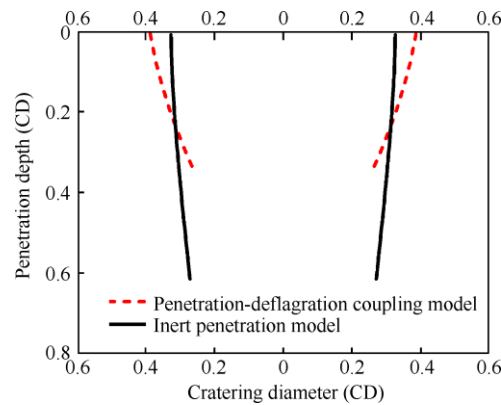


Fig. 10. Calculated penetration hole morphology using inert penetration mode and penetration-deflagration coupling mode.

The weakening effect of the penetration-induced chemical response on the penetration capacity can be analyzed as follows. According to the penetration theory [26], for a penetrator with a given initial velocity, the penetration capability mainly depends on its density and length. The higher the density, the higher the penetration velocity, and the larger the penetration depth. The longer the length, the longer the penetration time, and the larger the penetration depth. However, the penetration process of reactive penetrator is accompanied by a chemical response, which causes changes of the density and length of each reactive element at the time of impact, thus resulting in a change of penetration capability. On the one hand, there is a chemical reaction zone near the impact interface, which causes the reactive element to experience a certain degree of chemical reaction before impacting the plate, resulting in a decrease of its density and penetration velocity, see Figs. 11(a) and 11(b). As a result, its penetration capability is weakened. On the other hand, due to the decreased penetration velocity, the elongation effect of reactive elements during penetration is weakened (see Fig. 11(c)), resulting in a decrease of penetration time. This further weakens its penetration capability. Therefore, the penetration-induced chemical response is unfavorable to penetration.

The enhancement effect of the penetration-induced chemical response on cratering capability can be analyzed as follows. According to the cratering theory [25,26], the cratering capability of penetrator mainly depends on its diameter and radial cratering pressure, and both are positively correlated. As mentioned above, the penetration-induced chemical response causes a decreased reactive element density and penetration velocity, as well as a weakened elongation effect, thus resulting in a weakened penetration capability. On the contrary, the weakened elongation effect means that the diameter of reactive element at the time of impact increases (see Fig. 11(d)), which causes more significant deformation and stacking effects at the bottom of the hole, resulting in an enhanced cratering capability. Furthermore, the cratering pressure is increased due to the deflagration reaction, which further enhances its cratering capability. Therefore, the penetration-induced chemical response is favorable to cratering.

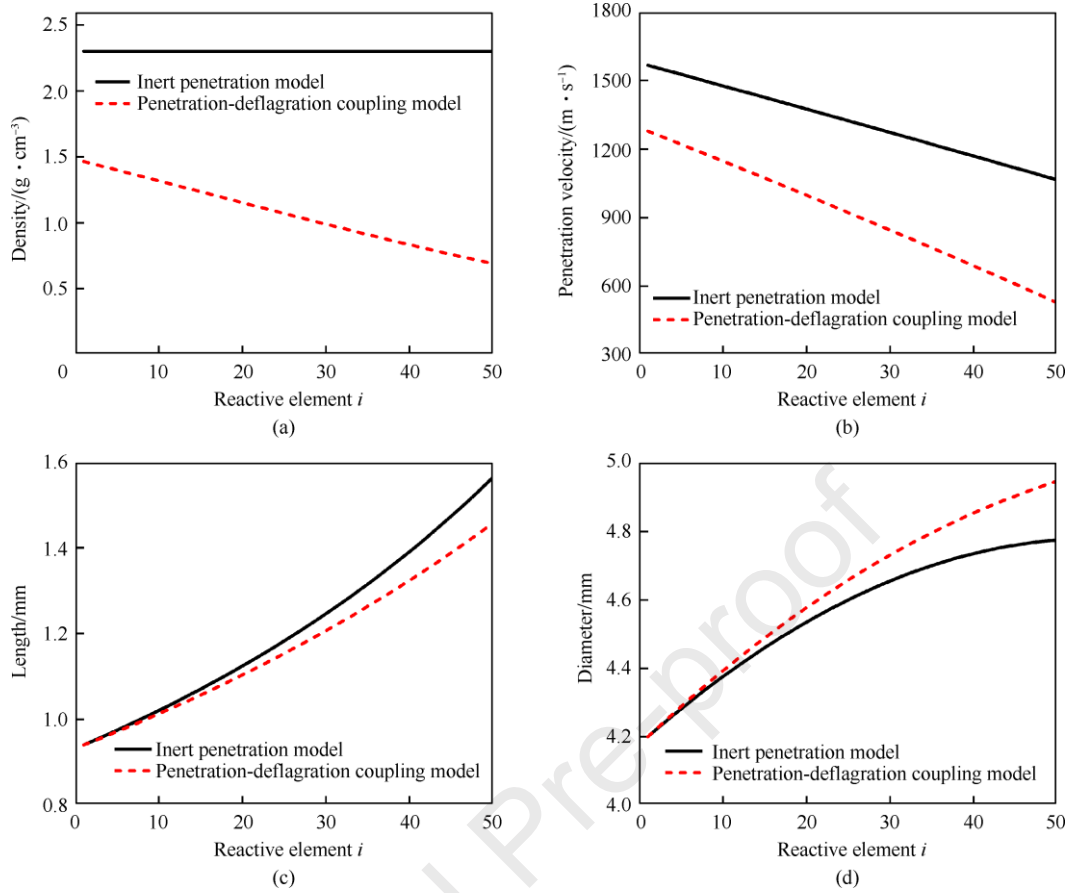


Fig. 11. Performance parameters of reactive elements at the time of impact in inert penetration mode and penetration-deflagration coupling mode: (a) Density; (b) Penetration velocity; (c) Length; (d) Diameter.

4.3. Influence of reactive liner density

Both experimental and calculated results show that with the increase of reactive liner density, the penetration capability is significantly enhanced, but the cratering capability is significantly weakened, see Table 4 and Fig. 9. In this section, based on the developed penetration-deflagration model, the influence of reactive liner density on the penetration-deflagration performance is analyzed from the three aspects of the formation characteristics, the penetration effect and the penetration-induced chemical response behavior.

From the formation characteristics, as the reactive liner density increases, the formation velocity of reactive penetrator decreases, but its velocity gradient does not change much, see Table 3. This results in a more sufficiently free elongation of the reactive penetrator before impacting plate, which is favorable to penetration. On the contrary, the more sufficiently free elongation means a more significant diameter shrinkage effect, resulting in a decreased diameter of reactive penetrator at the time of impact, which is unfavorable to cratering.

From the penetration effect, as the reactive liner density increases, the kinetic

energy of reactive penetrator shows an increasing trend. This results in an increasing penetration velocity of each reactive element (see Fig. 12), which is favorable to penetration. However, the enhanced penetration capability means a more sufficient elongation of reactive penetrator during penetration, resulting in a decreased diameter of reactive element at the time of impact, which is unfavorable to cratering.

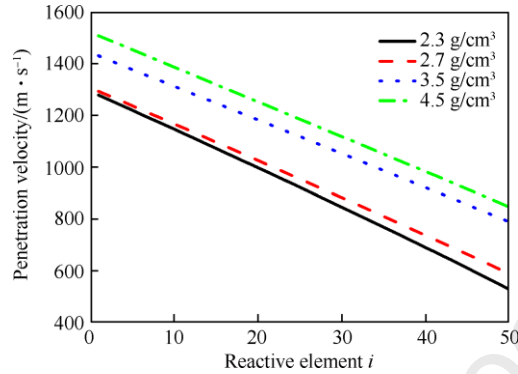


Fig. 12. Penetration velocity of each reactive element under different reactive liner densities.

From the penetration-induced chemical response behavior, the increase of Al-PTFE-Cu reactive material density usually means the decrease of energetic composition Al-PTFE and the increase of high-density inert metal composition Cu. In other words, the energetic composition participating in the chemical reaction decreases as the reactive liner density increases, which causes that the weakened effect of the penetration-induced chemical response on the penetration capability is weakened, as shown in Fig. 13. Therefore, in terms of the influence degree of the penetration-induced chemical response, increasing the reactive liner density is favorable to penetration. On the contrary, the decreased energetic composition will cause a weakened cratering effect by the deflagration, resulting in a weakened cratering capability.

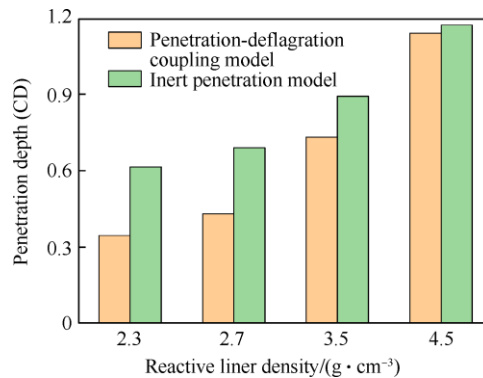


Fig. 13. Changing trend of penetration depth with reactive liner density in inert penetration mode and penetration-deflagration coupling mode.

Above all, increasing the reactive liner density not only significantly increases the kinetic energy and length of the reactive penetrator, but also effectively decreases the weakened effect of the penetration-induced chemical response on the penetration capability, resulting in the significantly enhanced penetration capability. However, the

cratering capability weakens significantly due to the decrease of reactive penetrator diameter at the time of impact and its own potential energy content.

5. Conclusions

Penetration-deflagration coupling damage performance of RRSCP impacting thick steel plates is investigated by experiments and theoretical model. The main findings are summarized as follows.

(1) The theoretical model for penetration-deflagration coupling damage performance is developed. The model-predicted penetration depth and cratering diameter are in good agreement with the experimental results, which can be used to quantitatively analyze the penetration-deflagration performance of RRSCP.

(2) The chemical response of reactive element near the impact interface is triggered by penetration, resulting in a decrease of its density at the time of impact, a decrease of its penetration velocity and a weakening of its elongation effect during penetration, which is unfavorable to penetration. However, the diameter of reactive penetrator impacting the plate is increased due to the weakened elongation effect, which coupled with the chemical energy release of deflagration, resulting in an enhanced cratering effect.

(3) Increasing the reactive liner density significantly increases both the kinetic energy and length of reactive penetrator and effectively reduces the weakened effect of the penetration-induced chemical response, which significantly enhances the penetration capability. However, due to the decrease of reactive penetrator diameter at the time of impact and its own potential energy content, the cratering capability is weakened significantly.

Acknowledgments

This research is supported by the National Natural Science Foundation of China (Grant No. 12172052) and the Foundation of State Key Laboratory of Explosion Science and Safety Protection (Grant No. QKKT24-02).

References

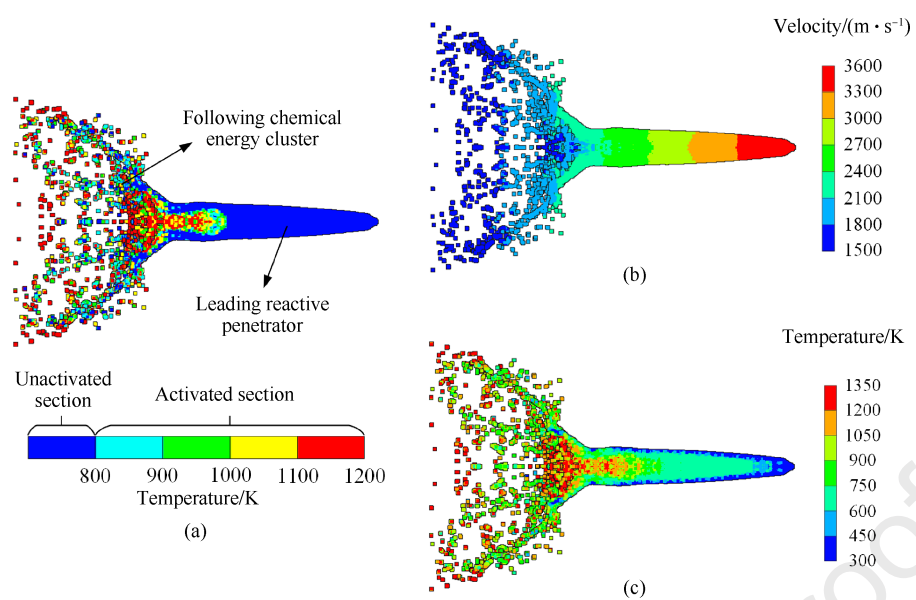
- [1] Wang YZ, Yu QB, Zheng YF, Wang HF. Formation and penetration of jets by shaped charges with reactive material liners. *Propellants Explos Pyrotech* 2016;41:618-22.
- [2] Daniels AS, Baker EL, DeFisher SE, et al. Bam: large scale unitary demolition warheads. 23 International Symposium on Ballistics, Tarragona, Spain, 2007, 16-20.
- [3] Baker EL, Daniels AS, Ng KW, et al. Barnie: a unitary demolition warhead. 19 International Symposium on Ballistics, Interlaken, Switzerland, 2001, 569-574.
- [4] Xiao JG, Zhang XP, Guo ZX, Wang HF. Enhanced damage effects of multi-layered concrete target produced by reactive materials liner. *Propellants Explos Pyrotech* 2018;43(9):955-61.
- [5] Zhang H, Zheng YF, Yu QB, Ge C, Su CH, Wang HF. Penetration and internal blast behavior of reactive liner enhanced shaped charge against concrete space. *Def Technol* 2022;18(6):952-62.

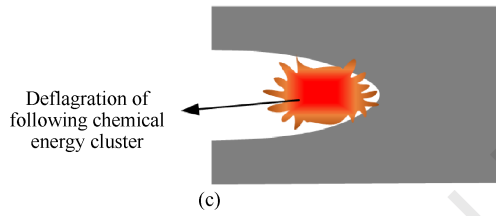
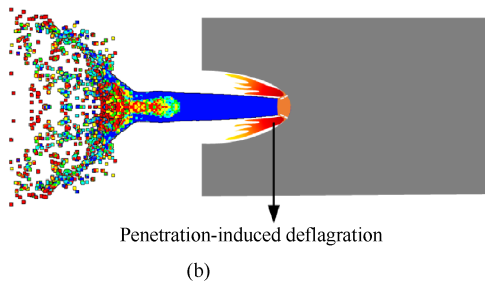
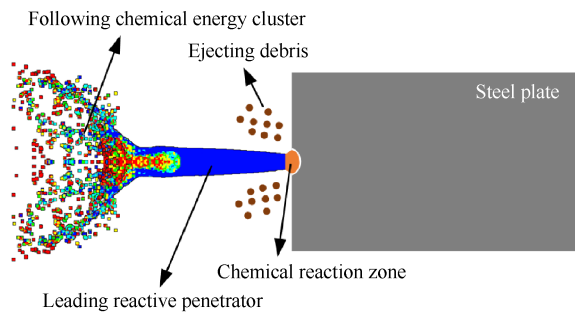
- [6] Zheng YF, Su CH, Guo HG, Yu QB, Wang HF. Behind-target rupturing effects of sandwich-like plates by reactive liner shaped charge jet. *Propellants Explos Pyrotech* 2019;44(11):1400-09.
- [7] Guo HG, Zheng YF, Yu QB, Ge C, Wang HF. Penetration behavior of reactive liner shaped charge jet impacting thick steel plates. *Int J Impact Eng* 2019;126:76-84.
- [8] Guo HG, Su CH, Cai YQ, He S, Yu QB, Wang HF. Reactive jet density distribution effect on its penetration behavior. *Def Technol* 2023;24(6):190-202.
- [9] Guo HG, Zheng YF, Tang L, Yu QB, Ge C, Wang HF. Effect of wave shaper on reactive materials jet formation and its penetration performance. *Def Technol* 2019;15(4):495-505.
- [10] Zheng YF, Su CH, Guo HG, Yu QB, Wang HF. Chain damage effects of multi-spaced plates by reactive jet impact. *Def Technol* 2021;17(2):393-404.
- [11] Guo HG, Xie JW, Wang HF, Yu QB, Zheng YF. Penetration behavior of high-density reactive material liner shaped charge. *Materials* 2019;12(21):3486.
- [12] Sun T, Wang HF, Wang SP, Ge C, Hu D, Chen PW. Formation behaviors of rod-like reactive shaped charge penetrator and their effects on damage capability. *Def Technol* 2024;32(2):242-53.
- [13] Sun T, Yuan Y, Zheng YF, Yu QB, Chen PW, Wang HF. The influences of liner shape on the formation of reactive shaped charge penetrator. *Transactions of Beijing Institute of Technology* 2024;44(4):327-335 (in Chinese).
- [14] Meyers MA. *Dynamic behavior of materials*. San Diego: University of California, 1994:98-117.
- [15] Verreault J. Analytical and numerical description of the PELE fragmentation upon impact with thin target plates. *Int J Impact Eng* 2015;76:196-206.
- [16] Liu JF, Long Y, Ji C, Zhong MS, Liu Q. The influence of liner material on the dynamic response of the finite steel target subjected to high velocity impact by explosively formed projectile. *Int J Impact Eng* 2017;109:264-75.
- [17] Reding DJ, Hanagud S. Chemical reaction in reactive powder metal mixtures during shock compression. *J Appl Phys* 2009;105(2):175-80.
- [18] Tang L, Wang HF, Lu GC, Zhang H, Ge C. Mesoscale study on the shock response and initiation behavior of Al-PTFE granular composites. *Mater Des* 2021;200:109446.
- [19] Losada M, Chaudhuri S. Theoretical study of elementary steps in the reactions between aluminum and teflon fragments under combustive environments. *J Phys Chem A* 2009;113(20):5933-41.
- [20] Liu SB, Zheng YF, Yu QB, Ge C, Wang HF. Interval rupturing damage to multi-spaced aluminum plates impacted by reactive materials filled projectile. *Int J Impact Eng* 2019;130:153-62.
- [21] Birkhoff G, MacDougall DP, Pugh EM, Taylor SG. Explosives with lined cavities. *J Appl Phys* 1948;19:563-82.
- [22] Rosenberg Z, Dekel E. A critical examination of the modified Bernoulli equation using two-dimensional simulations of long rod penetrators. *Int J Impact Eng* 1994;15(5):711-20.
- [23] Chen G, Chen ZF, Tao JL, Niu W, Zhang QP, Huang XC. Investigation and validation on plastic constitutive parameters of 45 steel. *Explos Shock Waves* 2005;25(5):451-56 (in

Chinese).

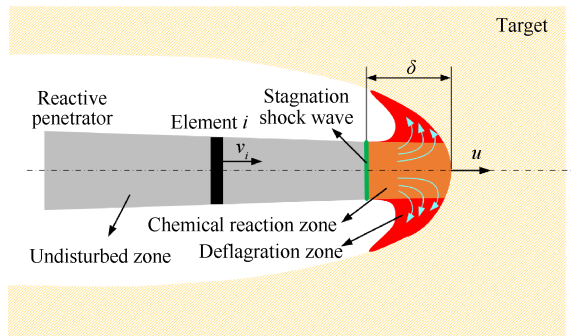
- [24] Xiao QQ, Huang ZX, Zhu CS, Zu XD. Calculation of depth and crater diameter for the supersonic penetration of shaped charge jet into concrete. *Propellants Explos Pyrotech* 2013;38(2):224-31.
- [25] Held M. Verification of the equation for radial crater growth by shaped charge jet penetration. *Int J Impact Eng* 1995;17(3):387-98.
- [26] Held M. Determination of the crater radius as a function of time of a shaped charge jet that penetrates water. *Propellants Explos Pyrotech* 1996;21:64-9.

Journal Pre-proof

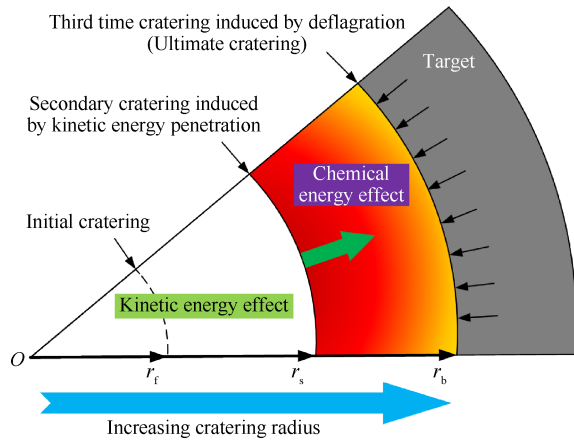


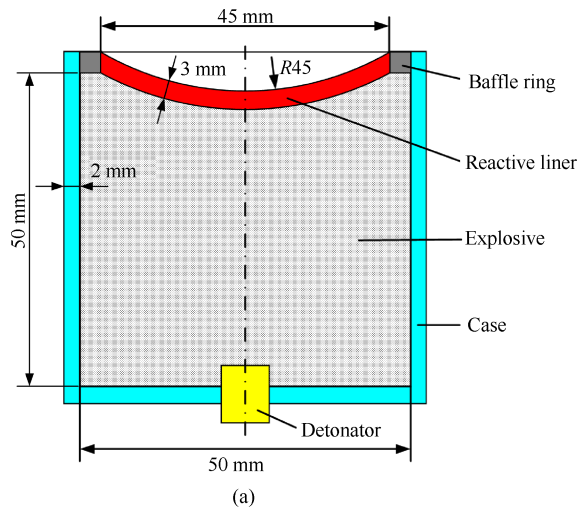


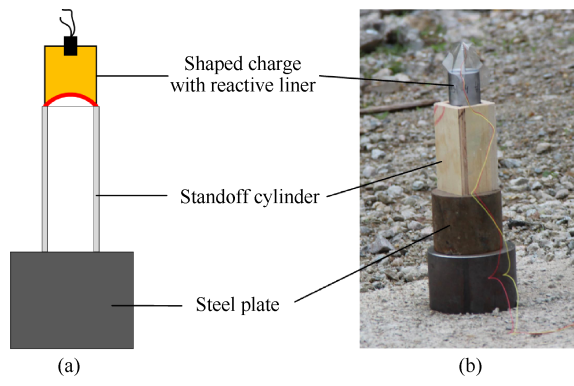
Journal Pre-proof



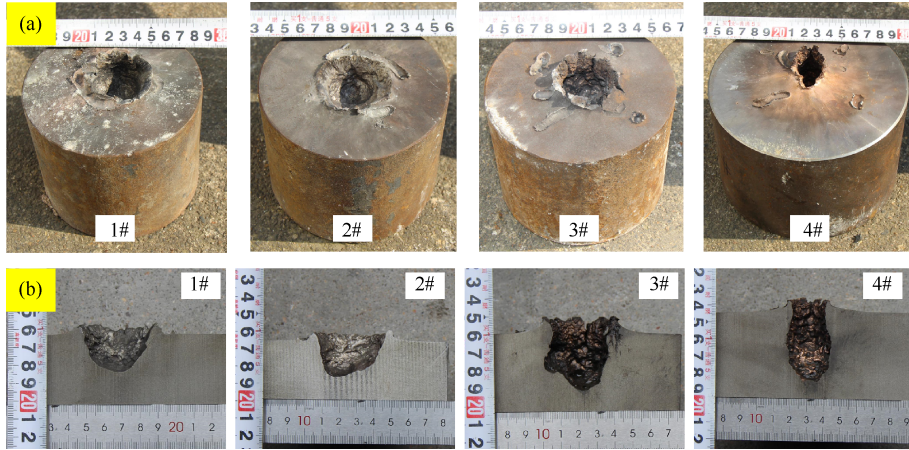
Journal Pre-proof



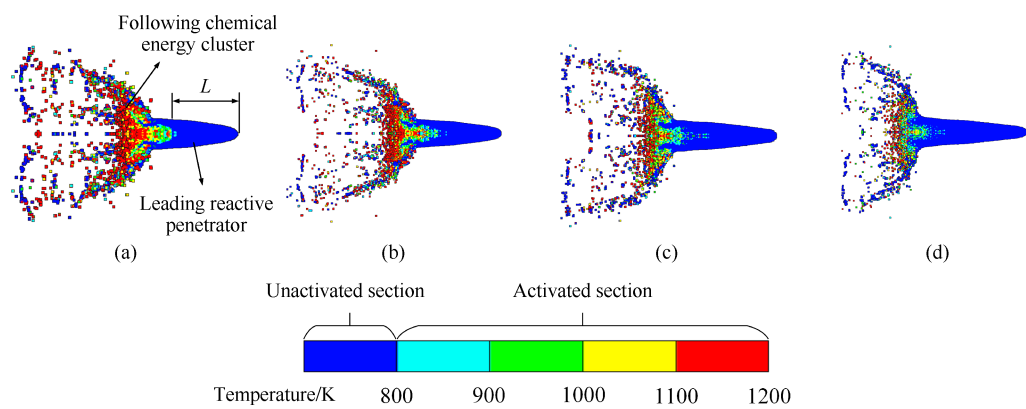


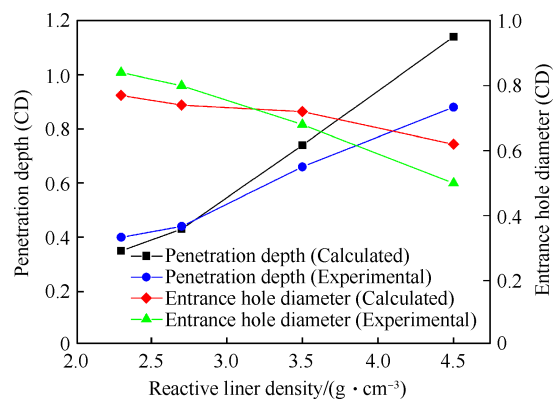


Journal Pre-proof

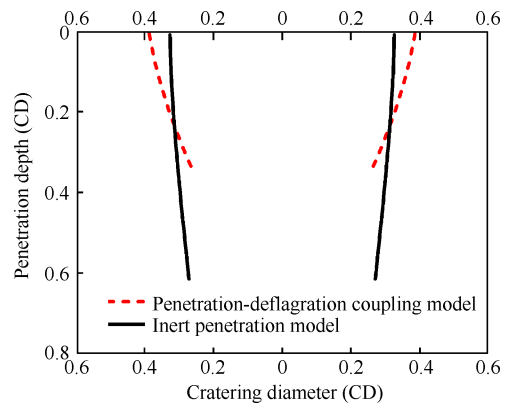


Journal Pre-proof

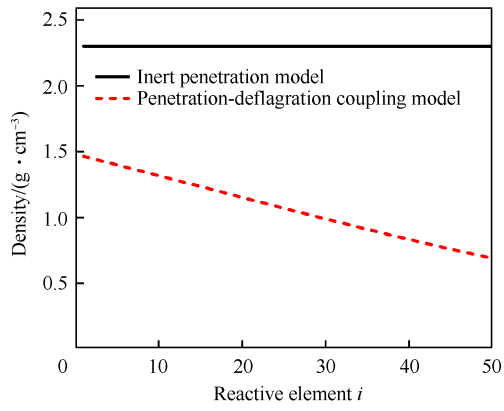




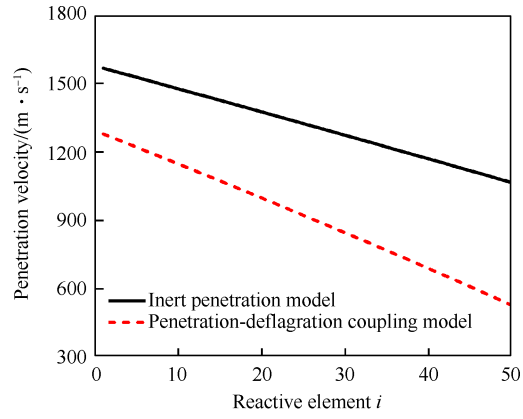
Journal Pre-proof



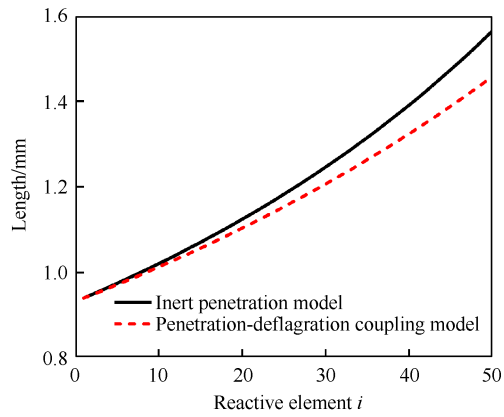
Journal Pre-proof



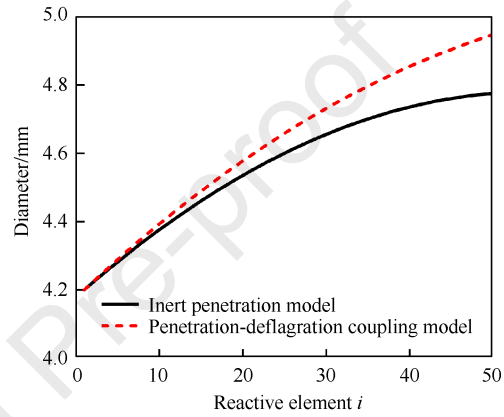
(a)



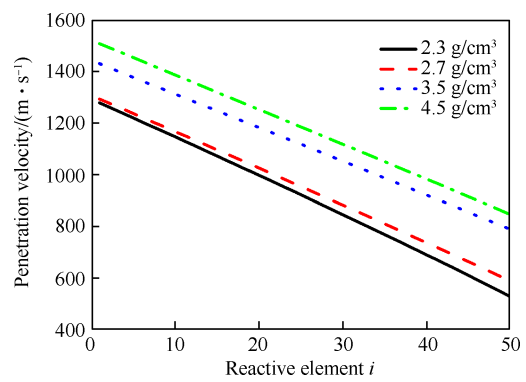
(b)



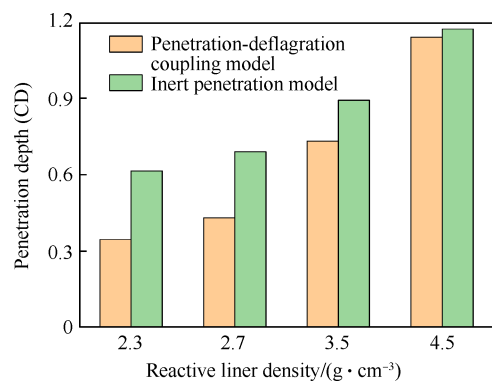
(c)



(d)



Journal Pre-proof



Journal Pre-proof

Highlights

- A theoretical model for the penetration-deflagration coupling damage performance of RRSCP is developed.
- The influence mechanism of penetration-induced chemical response on penetration and cratering capabilities is revealed.
- The influences of reactive liner density on the penetration-deflagration performance of RRSCP are discussed.

Declaration of interests

The authors declare that they have no known competing financial interests or personal relationships that could have appeared to influence the work reported in this paper.

The authors declare the following financial interests/personal relationships which may be considered as potential competing interests:

Journal Pre-proof